FASTER MAGNETIC FIELD COMPUTATION USING LOCALLY ORTHOGONAL DISCRETIZATION

Y. Saito, Y. Kishino, S. Hayano, H. Nakamura, N. Tsuya and Z. J. Cendes*

College of Engineering, Hosei University, Kajinocho Koganei
Tokyo 184, Japan
***Electrical and Computer Engineering Department,Carnegie Mellon University**
Pittsburgh, PA 15213

Abstract - Because of their simplicity and flexibility, first order triangular finite elements are the most widely used type of finite element in magnetic field computation. However, in the first order finite element procedure, a relatively large number of mesh points is required to obtain good solutions. In order to overcome this difficulty, we propose a new method of magnetic field computation based on locally orthogonal discretizations. Memory requirements and solution times are dramatically reduced by the new method.

INTRODUCTION

The application of complementary variational principles to magnetic field computation has been an active area of research in recent years.[1–5] Penman, Hammond, and their co-workers have employed complementary variational principles to obtain more accurate field values by averaging complementary solutions than is possible with one-sided methods;[1–3] Cendes and Shenton have employed complementary variational principles to determine local error bounds suitable for adaptive mesh refinement.[4–5] This work on complementary variational principles has been very valuable and has led not only to better magnetic field solutions but also to greater physical understanding. However, the dual finite element approach has a serious disadvantage: With this type of analysis, it is necessary to develop and to use two different variational principles and two different potential functions to generate the complementary solutions. This is sometimes a difficult and an expensive task.

In this paper, we present a new approach to generating complementary finite element solutions. Instead of utilizing the *physical duality* inherent in the complementary variational approach, we exploit the *geometric duality* inherent in some finite element discretization procedures. Indeed, we show that a geometric duality exists between Delaunay triangles and Voronoi polygons and that this duality provides natural complementary error bounds for finite element modeling. Since only one potential function is required with the geometric duality principle, the resulting solution procedure is considerably simpler and more efficient than the two potential approach. Further, the discretizations that result from the two geometric approximations may be directly averaged to form a highly efficient hybrid scheme. Computations show the hybrid discretization procedure to be approximately one order of magnitude more accurate than the standard first-order finite element scheme.

LOCALLY ORTHOGONAL DISCRETIZATIONS

Assumptions

Numerous problems in electrical engineering reduce to solving the Poisson equation in two dimensions

$$\lambda(\partial^2\phi/\partial x^2) + \lambda(\partial^2\phi/\partial y^2) = -\sigma, \tag{1}$$

where λ is a parameter depending on the medium, ϕ is a scalar or axial component of a vector, and σ is the source density. At the boundary between regions 1 and 2, the following boundary conditions are assumed:

$$\partial\phi/\partial\, y|_1 = \partial\phi/\partial y|_2 \tag{2}$$

$$\lambda_1(\partial\phi/\partial x)|_1 = \lambda_2(\partial\phi/\partial x)|_2 \tag{3}$$

The concept of Delaunay triangulation was introduced in finite element modeling by Cendes and Shenton.[4–6] In this procedure, the Delaunay triangulation of an arbitrary set of points is constructed by considering the properties of its geometric dual -- the set of Voronoi polygons. Delaunay triangles are related to Voronoi polygons in that the circumcenters of Delaunay triangles are the vertices of the Voronoi polygons.[4–6] An important property of Delaunay triangles is the fact that the distance between neighboring triangle circumcenters -- i.e. the lengths of the sides of the associated Voronoi polygons -- cannot be negative.

Figure 1(a) presents two triangles in a Delaunay mesh showing the centers k and l of the two triangle circumcircles. The Voronoi polygons associated with these triangles are shown by dashed lines in this figure. Further, each of the original triangles may be subdivided into two or three isosceles triangles by connecting the triangle circumcenters with the triangle vertices as shown by cross-hatched lines for one section of the triangles.

It is apparent that the Delaunay triangles and the Voronoi polygons formed in this way are locally orthogonal: each triangle side is perpendicular to the corresponding Voronoi polygon edge. In addition, two complete but independent sets of modal variables may be defined on this figure: one -- the primal set of variables -- are located at the vertices of the Delaunay triangles; the other -- the complementary set of variables -- are located at the vertices of the Voronoi polygons.

By adopting the local x-y coordinate system as shown in Figure 1(a) and by employing the piecewise linear approximation functions reported in Reference 7, it can be shown that Equation (1) reduces to a one-dimensional equation in either the primal or in the dual sets of variables

$$\lambda(\partial^2\phi/\partial y^2) = -(1/2)\sigma, \tag{4}$$

$$\lambda(\partial^2\phi/\partial x^2) = -(1/2)\sigma. \tag{5}$$

Functionals

On the local coordinate system shown in Figure 1(a), nodes i and j are located on the boundary between the regions 1 and 2. This means that the derivative $\partial\phi/\partial y$ is common to both regions 1 and 2 in Figure 1(a). Thereby, the functional for (2) and (4) is written as

$$F(\phi) = \int \lambda(\partial\phi/\partial y)^2 dxdy - \int \phi\sigma dxdy, \tag{6}$$

where the integrals are evaluated over the hatched regions in Figure 1(a).

On the other hand, nodes k and l are located on the x-axis in Figure 1(a). In this case, the derivative $\lambda(\partial\phi/\partial$ x) is common to both regions 1 and 2. This yields a complementary functional G(ϕ) for (3) and (5)

$$G(\phi) = -\int (1/\lambda)(\lambda\partial\phi/\partial x)^2 dxdy + \int \hat{\phi}\sigma dxdy \tag{7}$$

where $\hat{\phi}$ denotes the prescribed value of potential ϕ at nodes k and l and the integrals are again evaluated over the hatched regions in Figure 1(a).

Combining (6) with (7) leads to the hybrid functional H(ϕ)

$$H(\phi) = (1/2)[F(\phi) + G(\phi)] \tag{8}$$

Boundness

To show that the functional F(ϕ) in (6) reaches a minimum at the true solution of (4), let ϕ denote this true solution, and let ψ_p be some differentiable function that is non-zero in the hatched regions in Figure 1(a) and vanishes at the prescribed boundary nodes. The approximate functional F($\phi+\epsilon\psi_p$) is then written as

0018-9464/86/0900-1057$01.00

$$F(\phi+\epsilon\psi_p) = F(\phi) + \epsilon\int [2\lambda(\partial\phi/\partial y)(\partial\psi_p/\partial y) \quad (9)$$

$$- \psi_p \sigma]dxdy + \epsilon^2 \int\lambda(\partial\psi_p/\partial y)^2 dxdy$$

where ϵ is a numerical parameter. Extremizing (9) results in

$$\int [2\lambda(\partial\phi/\partial y)(\partial\psi_p/\partial y) - \psi_p \sigma]dxdy \quad (10)$$

$$=2\int\lambda\psi_p(\partial\phi/\partial y)dx-\int\psi_p[2\lambda(\partial^2\phi/\partial y^2)+\sigma]dxdy = 0$$

Since the last term on the right side of (9) is always positive, a minimum is reached when the parameter ϵ is zero. In other words, $F(\phi)$ in (6) is a primal functional.

Similarly, by means of (7), the approximate functional $G(\phi+\epsilon\psi_c)$ is written as

$$G(\phi+\epsilon\psi_c) = G(\phi) - \epsilon\int [2\lambda(\partial\phi/\partial x)(\partial\psi_c/\partial x) \quad (11)$$

$$- \psi_c \sigma]dxdy - \epsilon^2 \int\lambda(\partial\psi_c/\partial x)^2dxdy$$

where ψ_c is some differentiable function that is non-zero in the hatched regions in Figure 1(a) and vanishes at the prescribed boundary nodes. Extremizing (11) results in

$$\int [2\psi(\partial\phi/\partial x)(\partial\phi_c/\partial x)-\psi_c \sigma]dxdy=2\int\lambda\psi_c(\partial\phi/\partial x)dy \quad (12)$$

$$-\int\psi_c[2\lambda(\partial^2\phi/\partial x^2)+\sigma]dxdy=0$$

Since the last term on the right side of (11) is always negative, the functional $G(\phi+\epsilon\psi_c)$ in (11) will be a maximum when the parameter ϵ is zero. Thus $G(\phi)$ in (7) is a complementary functional. It follows that minimizing (9) yields the upper bound solutions, and maximizing (11) yields the lower bound solutions.[8] We therefore conclude that the approximate solutions ϕ_p obtained by using (9) are greater than the exact solution ϕ but that the approximate solutions ϕ_c obtained by using (11) are smaller than the exact solution ϕ

$$\phi_p = \phi + \epsilon\psi_1 \quad (13)$$

$$\phi_c = \phi - \epsilon\psi_2 \quad (14)$$

Here ψ_1 and ϕ_2 are differentiable functions that are non-zero in the hatched regions in Figure 1(a) and vanish at the prescribed boundary nodes.

By means of (6)-(14), it follows that the hybrid functional is bounded

$$F(\phi_p) \geqq HYBRID\ FUNCTIONAL \geqq G(\phi_c) \quad (15)$$

Convergence

When (13) and (14) are introduced into (6) and (7) respectively, the extremization of the hybrid functional (8) yields

$$\delta H = \lim_{\epsilon \to 0} (1/2\epsilon)[<F(\phi_p)-F(\phi)>+<G(\phi_c)-G(\phi)>] = 0 \quad (16)$$

Equation (16) results in the following relationships:

$$\int\lambda\psi(\partial\phi/\partial y)dx+\int\lambda\psi(\partial\phi/\partial x)dy=0, \quad (17)$$

$$\int\psi[\lambda(\partial^2\phi/\partial y^2)+\lambda(\partial^2\phi/\partial x^2)+\sigma]dxdy=0. \quad (18)$$

Equations (17) and (18) prove that extremizing the hybrid functional provides correct solutions to Equation (1).

The convergence of the numerical solution is accelerated by averaging the approximate solutions in (13) and (14). For example, the mid-side potential ϕ_a in Figure 1(a) is given by

$$\phi_a = (1/2)(\phi_i + \phi_k). \quad (19)$$

The average potential ϕ_a in (19) has higher accuracy than either ϕ_i or ϕ_k since the nodal potential ϕ_i is determined from the primal functional while the potential ϕ_k is determined from the complementary functional. Provided that $\psi_1\approx\psi_2$, the term $\epsilon\psi$ in (13) and (14) is therefore canceled by using the interpolation process in (19).

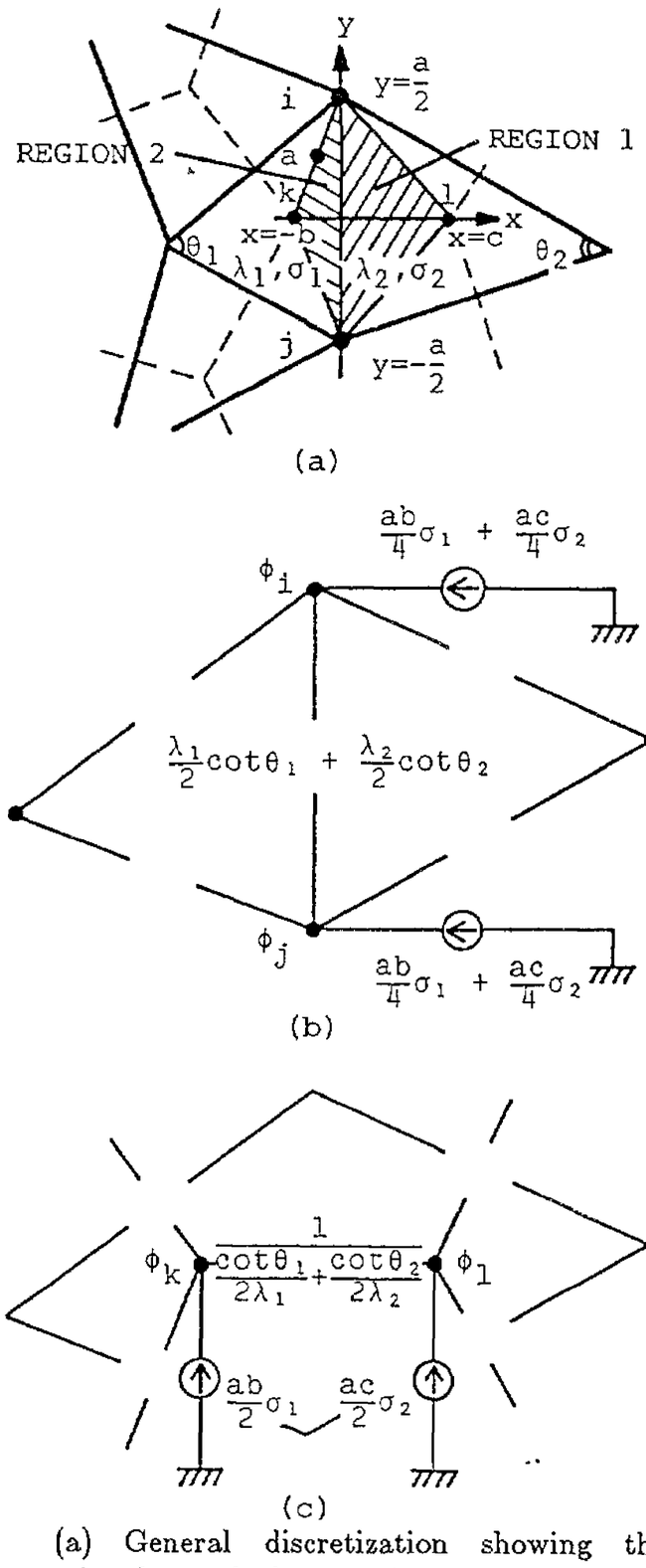

Figure 1. (a) General discretization showing the Delaunay triangles and the associated Voronoi polygons. The nodes for the primal variables are located at the triangle vertices, while the nodes for the complementary variables are located at the circumcenters of the Delaunay triangles. (b) The primal network between the nodes i and j in the subregion of Figure 1(a). (c) The complementary network between the nodes k and l in the subregion of Figure 1(a).

Node Equations

Introducing a simple linear Lagrange interpolation between nodes i and j in Figure 1(a) provides the following trial function for the primal functional

$$\phi_p=(1/2)(\phi_i+\phi_j)+(\phi_i-\phi_j)(y/a). \quad (20)$$

Note that this approximation function satisfies the boundary conditions (2).

Substituting (20) into (6) and minimizing the result yields discretized forms For example, for node i in Figure 1(a) the result is

$$\partial F(\phi_p)/\partial\phi_i=[(\lambda_1/2)cot\theta_1+(\lambda_2/2)cot\theta_2](\phi_i-\phi_j) \quad (21)$$

$$-(1/4)(ab\sigma_1+ac\sigma_2) = 0.$$

Equations for the other nodes in the primal system are obtained in the same way. The full set of node equations gives the primal network shown in Figure 1(b). It is interesting to note that the network parameters in Figure 1(b) coincide with those produced by the first order finite element method.[9]

The trial function ϕ_c for complementary functional must satisfy boundary condition (3). In order to satisfy this condition, we must employ two different trial functions given by

$$\phi_c=[(\lambda_1/b)\phi_k+(\lambda_2/c)\phi_1]/[(\lambda_1/b)+(\lambda_2/c)] \quad (22a)$$
$$+[(\lambda_2/bc)(\phi_1-\phi_k)]x/[(\phi_1/b)+(\lambda_2/c)]$$

$$\phi_c=[(\lambda_1/b)\phi_k+(\lambda_2/c)\lambda_1]/[(\lambda_1/b)+(\lambda_2/c)] \quad (22b)$$
$$+[(\lambda_1/bc)(\phi_1-\phi_k)]x/[(\lambda_1/b)+(\lambda_2/c)l$$

Equations (22a) and (22b) apply within the regions 1 and 2, respectively, in Figure 1(a). Introducing (22a) and (22b) into (7) and maximizing the result yields the discretized form. For example, for node k in Figure 1(a) the result is

$$\partial G(\phi_c)/\partial\phi_k=(\phi_1-\phi_k)/[(1/2\lambda_1)cot\theta_1 \quad (23)$$
$$+(1/2\lambda_2)cot\theta_2]+(ab/2)\sigma_1=0.$$

Equations for the other nodes in the complementary system are obtained in the same way. The full set of node equations gives the complementary network shown in Figure 1(c).

An Example

To illustrate the method, we applied it to the calculation of the magnetic field in ferromagnetic material of square cross-section. This example has been used by Hammond and Tsiboukis for demonstrating the dual finite element method.[2]

By symmetry, only part of the square must be computed as shown in Figure 2. In this example, ϕ,λ and σ of Equation (1) correspond to the axial component of the vector potential, inverse permeability, and current density, respectively.

Figure 3 shows the results of computations obtained by the new method, as well as results obtained by using the first order finite element method. As is evident from Figure 3, the use of either the primal or the complementary network system is inferior to the conventional first order finite element method. However, the hybrid method based on averaging the primal and complementary systems is far superior to the conventional first order finite element method and provides nearly an order of magnitude improvement in accuracy for a given number of nodes.

Figure 4 provides a comparison of the equipotential lines obtained by means of the hybrid method and by the first order finite element method for a small mesh (N=10). While the solution generated by the finite element method departs significantly from the analytical solution with this coarse mesh, the solution produced by the hybrid method is quite accurate. Thus the local orthogonal discretization procedure provides excellent potential distributions even with extremely small meshes.

CONCLUSIONS

A new method of computing two dimensional magnetic fields has been developed. The method is based on the geometrical duality of Delaunay triangles and Voronoi polygons. Since these geometric structures are locally orthogonal, they provide complementary solutions without the complications engendered by dual energy-dual potential methods.

To obtain solutions of similar accuracy in an example problem, the new method required about one-tenth of the nodes and considerably less computer time than the conventional first order finite element method.

REFERENCES

1. Penman, J. and J.R. Fraser, "Complementary and Dual Energy Finite Element Principles in Magnetostatics," *IEEE Transactions on Magnetics, Vol. MAG-18*, No. 2, March 1982, pp. 319-324.

2. Hammond, P. and T.D. Tsiboukis, "Dual Finite-Element Calculations for Static Electric and Magnetic Fields," *Proc. IEEE, Pt. A, Vol. 130*, No. 3, May 1983, pp. 105-111.

3. Hammond, P. and J. Penman, "Calculation of Inductance and Capacitance by Means of Dual Energy Principles," *Proc. IEEE, Vol. 123*, No. 6, June 1976, pp. 554-559.

4. Cendes, Z.J., D.N. Shenton and H. Shahnasser, "Magnetic Field Computation Using Delaunay Triangulation and Complementary Finite Element Methods," *IEEE Transactions, Vol. MAG-19*, 1983, pp. 2551-2554.

5. Cendes, Z.J. and D.N. Shenton, "Complementary Error Bonds for Foolproof Finite Element Mesh. Generation," *Mathematics and Computers in Simulation, Vol. 27*, 1985, pp. 295-305.

6. Shenton, D.N. and Z.J. Cendes, "Three-Dimensional Finite Element Mesh Generation Using Delaunay Triangulation," *IEEE Transactions, Vol. MAG-21*, 1985, pp. 2535-2538.

7. Saito, Y., et al, "Field Computations by the Complementary Networks," *IEEE Trans., Magnetics*, in printing.

8. Finlayson, B.A., *The Method of Weighted Residuals and Variational Principles*, Academic Press, New York, 1972.

9. Silvester, P.P. and R.L. Ferrari, *Finite Elements for Electrical Engineers*, Cambridge University Press, Cambridge, 1983.

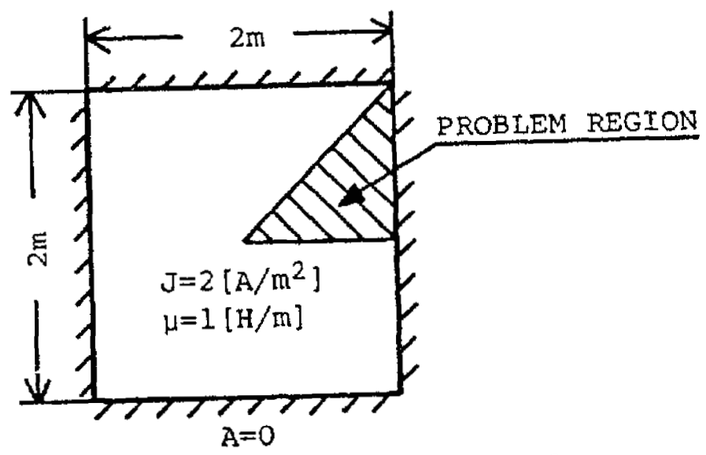

Figure 2. A highly permeable conductor of square cross-section analyzed in [2].

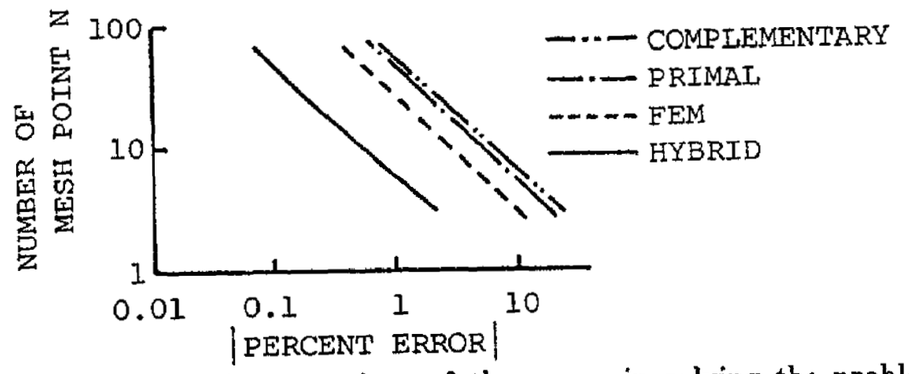

Figure 3. A comparison of the errors in solving the problem in Figure 2 expressed in terms of the absolute values of error in the functionals.

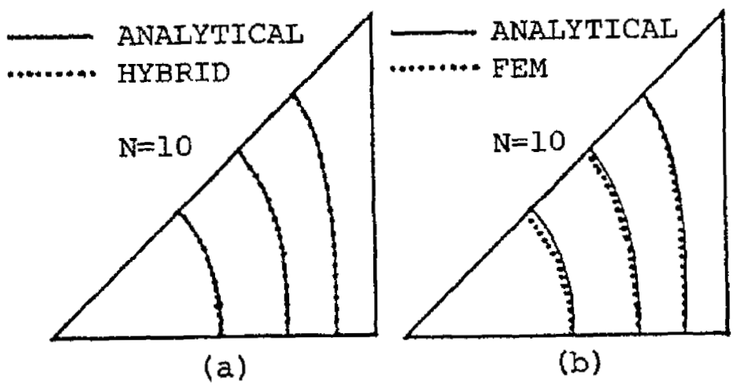

Figure 4. Equipotential lines for the problem in Figure 2. (a) The dotted lines were produced by the local orthogonal discretization method. (b) The dotted lines were produced by the conventional first order finite element method.